ELSEVIER

Thermochimica Acta 262 (1995) 13–31

thermochimica acta

Polymerization calorimeter. Part 1. Modelling and characterization

Mikko Lahti [a,*], Arno Avela [b], Jukka Seppälä [a]

[a] *Helsinki University of Technology, Department of Chemical Engineering Laboratory of Industrial Chemistry and Polymer Technology, Kemistintie 1, FIN-02150 Espoo, Finland*

[b] *Borealis Polymers Oy, R & T, FIN-06101 Porvoo, Finland*

Received 14 September 1994; accepted 15 March 1995

Abstract

An understanding of calorimeter design as applied at low temperatures (50–70°C) was used to construct a heat balance calorimeter that is also suitable for high-temperature applications (90–120°C). The broad temperature scale means that a wide range of polyreactions can be studied. An accurate model for the thermal effects of the reaction calorimeter is needed to ensure good estimates of basic parameters and to guarantee an accurate characterization of its operation. The time constants of the temperature measurement devices and the heat capacities of the system parts were carefully determined in simulated reactions. The dynamic behaviour of the calorimeter is well described by the five differential equations presented.

Keywords: Dynamic modelling; Heat balance calorimeter; Polymerization calorimeter; Reaction calorimetry; Thermal modelling

List of symbols

A/m^2	heat transfer area
$c_p/\mathrm{kJ\ kg^{-1}\ K^{-1}}$	heat capacity of the cooling liquid
d/m	diameter of the stirrer
D/m	diameter of the reactor
$h_i/\mathrm{W\ m^{-2}\ K^{-1}}$	inside heat transfer coefficient of the reactor
$h_o/\mathrm{W\ m^{-2}\ K^{-1}}$	jacket-side heat transfer coefficient of the reactor

* Corresponding author.

SSDI 0040-6031(95)02352-6

k	coefficient which depends on the reactor geometry and physical properties
K_p/W K^{-1}	heat transfer coefficient
M_t/N m	stirrer torque
$\dot{m}$/kg s^{-1}	mass flow rate of the cooling liquid
N/s^{-1}	agitation rate
$\dot{Q}_c$/W	power input by the heater
$\dot{Q}_{cond}$/W	conductive heat flow rate
$\dot{Q}_{conv}$/W	convective heat flow rate
$\dot{Q}_{diss}$/W	power input by the stirrer
$\dot{Q}_{elect}$/W	power input by the electrical heater
$\dot{Q}_r$/W	heat flow rate by reaction
$\dot{Q}_{pump}$/W	power input by the gear pump
$\dot{Q}_{sec}$/W	secondary heat flow rate effects
s/m	thickness of the reactor wall
T_j/K	jacket temperature
T_{j0}/K	jacket inlet temperature
T_p/K	pump head temperature
T_{PT100}/K	temperature of the jacketed probe
T_r/K	reactor temperature
T_w/K	temperature after the heat exchanger
U/W m^{-2} K^{-1}	overall heat transfer coefficient
u/V	analogue input
$\Sigma(mc_p)_{const,j}$/J K^{-1}	heat capacity of the jacket which is due to the mass of the jacket construction
$\Sigma(mc_p)_{const,r}$/J K^{-1}	heat capacity of the reactor which is due to the mass of the reactor construction
$\Sigma(mc_p)_e$/J K^{-1}	heat capacity of the electrical heater
$\Sigma(mc_p)_j$/J K^{-1}	heat capacity of the jacket
$\Sigma(mc_p)_r$/J K^{-1}	heat capacity of the reactor

Greek letters

λ/W m^{-1} K^{-1}	thermal conductivity of the reactor wall
ρ/kg m^{-3}	density
η/Pa s	viscosity
Ψ/m^2 K W^{-1}	sum of the wall and jacket side film resistances
τ_{PT100}/s	time constant of the probe
τ_{T_p}/s	time constant of the head of the gear pump

1. Introduction

Calorimeters are used to estimate thermal effects associated with chemical reactions. The reaction calorimeter is a powerful tool for on-line determination of polymerization

rate and monomer conversion in batch and semi-batch polymerizations. For batch polymerizations in particular, the reaction calorimeter offers the possibility of studying the mechanisms of the polymerization process.

Thermal modelling of the reaction calorimeter ensures good estimates of basic parameters and guarantees accurate characterizations of the device. The dynamic behaviour of bench-scale reaction calorimeters has been studied earlier [1–4].

The reaction calorimeter was characterized and tested for the temperature range 60–120°C. The upper limit for the temperature is 150°C because this is the maximum operating temperature of the heat transfer medium. When temperatures are high, calorimetric measurements are, of course, affected by the heat losses but the effects can be minimized by carefully characterizing all the possible heat flows to and from the system. The broad temperature scale means that a wide range of polyreactions can be studied.

2. Experimental apparatus

An apparatus was developed for studying different types of polymerizations by calorimetry. Batch and semi-batch polymerization can be studied.

A schematic presentation of the apparatus is shown in Fig. 1. The polymerization reactor **a** is an autoclave 2 dm^3 in volume. The reactor is installed in an air-bath **b**, where the temperature is thermostated to the jacket temperature to avoid heat losses. This is done by using an electrical heater **m**. The flow rate in the inner circulation jacket loop **c** is high (approximately 0.2 $dm^3\ s^{-1}$) because this provides a good dynamic behaviour of the inner jacket loop and very small heat transfer resistance on the jacket side. The heat transfer medium is oil. The inner circulation jacket loop and the head of the gear pump **d** are also housed in the air-bath. In the outer circulation jacket loop **e**, there is a gear pump **h**. The flow rate of this pump is set to be constant, but it can be changed if the temperature control of the reactor is too slow. The flow rate in the outer loop is approximately 0.022 $dm^3\ s^{-1}$. In the outer circulation jacket loop there are also the heat exchanger **f** and the electrical heater **g**, which control the jacket inlet temperature T_{j0}. The temperature after the heat exchanger T_w is held constant by a thermostat which is coupled to the heat exchanger. The cooling liquid is then heated by an electrical heater **g** to the desired temperature which depends on the reactor temperature. Monomers are stored in pressurized vessels **k** and dosed to the reactor by pressure control units, **i** and **j**. Liquid reactants are dosed from the storage **o** to the reactor using the diaphragm pump **n**. The diaphragm pump is controlled according to the process concerned. The scales **p** record the amounts of the reactants added to the reactor. The data acquisition and most of the instrument control are handled by a personal computer **l**. It is essential to have a thermostated reactor lid **q** when the reactor has a large heat capacity. The dynamic response of the calorimeter is adversely affected by the heavy construction of the reactor and a thermostated reactor lid essentially improves the response.

The most important demand of heat balance calorimetry is a temperature measurement system of utmost precision. The system used in this study is based on

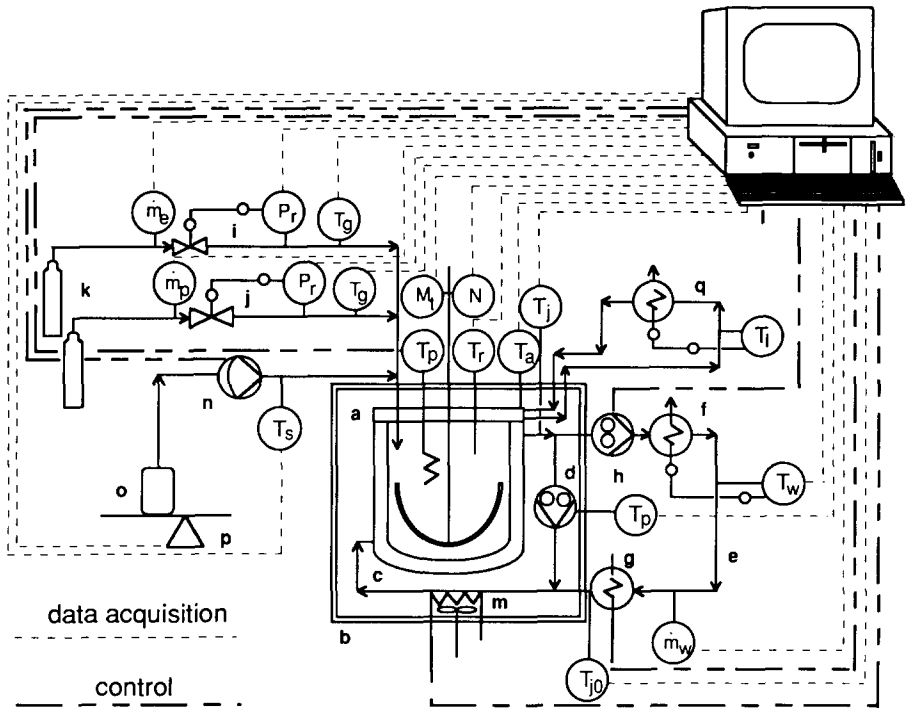

Fig. 1. Schematic presentation of the polymerization calorimeter: **a**, reactor; **b**, air-bath; **c**, inner circulation jacket loop; **d**, gear pump; **e**, outer circulation jacket loop; **f**, heat exchanger; **g**, electrical heater for heat transfer medium; **h**, gear pump; **i**, reactor pressure control; **j**, reactor pressure control; **k**, pressurized monomer storage; **l**, PC; **m**, electrical heater for air bath; **n**, diaphragm pump; **o**, monomer storage for liquid monomers; **p**, scales; **q**, thermostated loop for reactor lid.

commercially available solutions. The resolution of the temperature measurements is only 0.024°C due to the 12-bit A/D converter and the wide temperature range from 20 to 120°C; this can be improved by mathematical treatment, by using a high data acquisition rate and filtering the temperature signals. The accuracy of the temperature sensors is improved through calibration. For the purposes of the calibration, temperature sensors were placed in a thermostat (Lauda U 12) for 6 h at six temperatures from 80 to 120°C. Within this range, the sensors showed good linearity and the acquired voltages were scaled to engineering units with a linear function.

3. Characterization of the apparent viscosity measurement

In the determination of viscosity, changes in torque and agitation rate are used to calculate the stirrer power from which the Newton number, Ne, and subsequently the

Reynolds number, Re, are calculated. The Ne and Re numbers are then plotted on a diagram. Once this characteristic curve has been plotted, the viscosity is determined according to Eq. (3).

The power input by the stirrer $\dot{Q}_{diss}$ is calculated according to [5]

$$\dot{Q}_{diss} = 2\pi N M_t \tag{1}$$

from which the Newton number follows

$$Ne = \frac{\dot{Q}_{diss}}{\rho N^3 d^5} \tag{2}$$

The Reynolds number is then determined from the characteristic curve. From the Reynolds number, the viscosity can be calculated according to

$$\eta = \frac{\rho N d^2}{Re} \tag{3}$$

This method cannot be applied in the turbulent flow region because the Newton number is only a function of the Reynolds number when $Re < 10000$. Beyond that value, the Newton number becomes independent of the Reynolds number.

The characteristic curve was determined empirically. Different viscosity test standards were stirred with a specific stirrer used in a specific speed range, and the torque was read. The torque measuring system was the IKAVISC measuring stirrer, model MR-D. The determination of the characteristic curve for the used stirring system was done with glycerine/water mixtures with viscosity ranging from 40 to 1327 mPas and density from 1.21 to 1.26 g mol^{-1}. Three different volumes of the mixture were used (1.6, 1.7 and 1.8 dm^3) and four different stirrer speeds (3.3, 5.0, 6.7 and 8.3 s^{-1}). A correlation between the torque and the stirrer speed was made in the empty reactor before the characterization. The zero torque, which was strongly dependent on the stirrer speed, was due to only the mass of the magnet coupling and the friction between the bearings in the coupling. The zero torque was eliminated in the determination of the characteristic curve for the stirrer and only the true values were used in the characterization. The range of Newton numbers was 0.7–4.0 and the range of Reynold numbers was 20–1600. The characteristic curve for the stirrer is shown in Fig. 2. It is independent of the fill ratio of the reactor. The characteristic curve is fitted by the least squares method and corresponds to

$$Ne = 6.956 \times Re^{-0.284} \tag{4}$$

Statistical information about the curve fit performed is estimated according to the magnitude of the residuals ($R = 0.96$). Fig. 2 shows the relatively good fit.

The sensitivity of the measuring system is shown in Fig. 3. For this particular characterization, the lower limit of the sensitivity is approximately 10 N cm and the upper limit is 1500 N cm. The deviation in the determination of the viscosity is approximately $\pm$ 5% of the measured value.

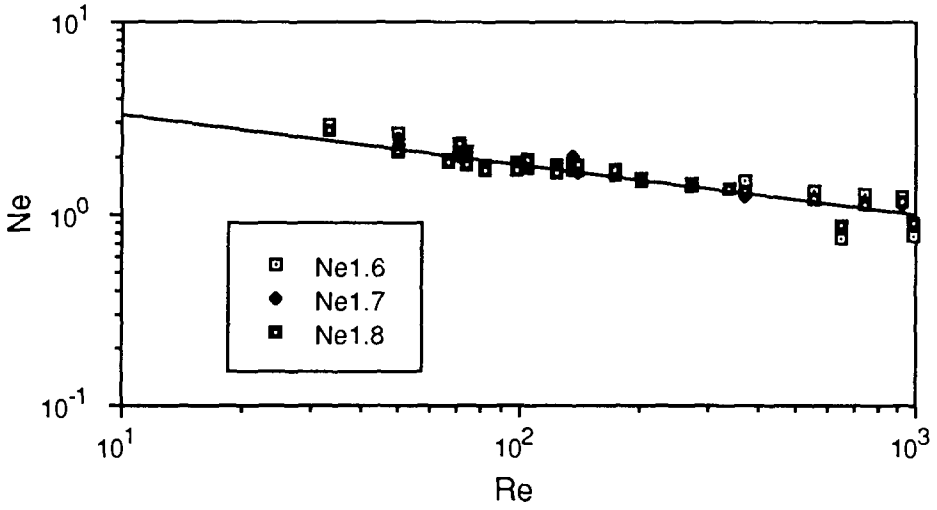

Fig. 2. Characteristic curve for the stirring system.

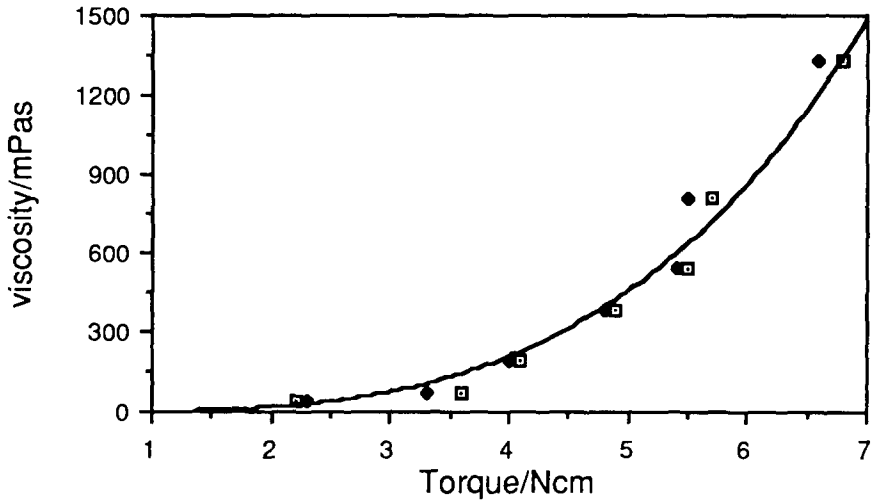

Fig. 3. Sensitivity of the viscosity measuring system.

4. Thermal modelling of the polymerization calorimeter

For simulation, a model of the reaction calorimeter is developed. The model includes the differential equations of the five temperatures that are important for a description of the dynamic behaviour of the calorimeter. The differential equations are based on the heat balance of the reactor and the heat balance of the jacket. The dissipated heat of the pump installed in the calorimeter, the temperature control algorithm, the heat capaci-

ties of the calorimeter and the time constants of the temperature measurement devices must be determined in the modelling. The simulation program is based on the program SIMULA which Moritz [1] developed for studying the dynamic behaviour of a laboratory reactor. Poersch-Panke [2] later improved the program and now it has been implemented for the device shown above.

4.1. Model equations

The dynamic heat balance of the reaction temperature is derived from the thermal model of the calorimeter in Fig. 4. $\dot{Q}_c$ and $\dot{Q}_r$ are constant during the simulation, while $\dot{Q}_{diss}$ is dependent on the experimental conditions (agitation rate and the viscosity of the reaction mixture). The heat transfer properties are a function of the modelled temperatures. The heat capacity of the reactor is assumed to be constant. Eq. (5) shows the dynamic heat balance of the ractor temperature

$$\frac{dT_r}{dt} = \frac{\dot{Q}_r + \dot{Q}_{diss} + \dot{Q}_c - UA(T_r - T_j)}{\Sigma(mc_p)_r} \tag{5}$$

where $\dot{Q}_r$ is the heat flow rate by reaction (W), $\dot{Q}_{diss}$ the power input by the stirrer (W), $\dot{Q}_c$ the power input by the calibration heater (W), U the overall heat transfer coefficient (W m^{-2} K^{-1}), A the heat transfer area (m^2), T_r the reactor temperature (K), T_j the jacket temperature (K), and $\Sigma(mc_p)_r$ the heat capacity of the reactor (J K^{-1}).

The mass flow and the heat capacity of the jacket are assumed to be constant during the simulation. The power input by the gear pump $\dot{Q}_{pump}$ is dependent on the modelled variables. The heat capacity of the cooling liquid is a function of the jacket temperature. The heavy construction of the head of the gear pump affects the dynamic behaviour of

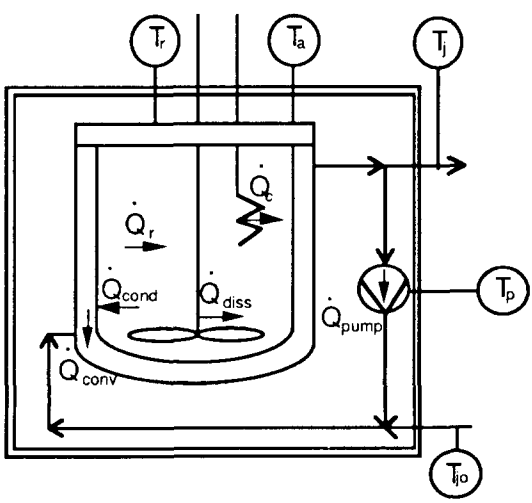

Fig. 4. Thermal model of the calorimeter.

the jacket temperature. There is quite a long time delay before the temperature of the pump head responds to the jacket temperature so that the heat flux through the pump head has to be modelled. The dynamic heat balance of the jacket temperature is shown in Eq. (6)

$$\frac{dT_j}{dt} = \frac{UA(T_r - T_j) + \dot{Q}_{pump} - \dot{m}(c_{pT_j} T_j - c_{pT_{j0}} T_{j0}) + K_p(T_j - T_p)}{\Sigma(mc_p)_j} \tag{6}$$

where $\dot{Q}_{pump}$ is the power input by the gear pump (W), $\dot{m}$ the mass flow rate of the cooling liquid (kg s^{-1}), c_p the specific heat capacity of the cooling liquid (kJ kg^{-1} K^{-1}), T_{j0} the jacket inlet temperature (K), K_p the heat transfer coefficient (W K^{-1}), T_p the pump head temperature (K), and $\Sigma(mc_p)_j$ the heat capacity of the jacket (J K^{-1}).

The mass flow rate and the heat capacity of the electrical heater are assumed to be constant during the simulation. The assumption that the temperature T_w is constant after the heat exchanger is valid for a steady state reaction, but may not be valid for modelling at the start of the simulation reaction when rapid changes in temperatures are occurring. $\dot{Q}_{elect}$ and the heat capacity of the cooling liquid are dependent on the modelled variables. The dynamic heat balance of the jacket inlet temperature is given by the equation

$$\frac{dT_{j0}}{dt} = \frac{\dot{Q}_{elect} + \dot{m}(c_{pTw} T_w - c_{pT_{j0}} T_{j0})}{\Sigma(mc_p)_e} \tag{7}$$

where $\dot{Q}_{elect}$ is the power input by the electrical heater (W), T_w the temperature after the heat exchanger (K), and $\Sigma(mc_p)_e$ the heat capacity of the electrical heater (J K^{-1}).

The temperature probe of the reactor is placed in a pocket which may cause time delay to the modelled temperatures. There is no essential time delay in the measurements of the jacket temperature T_j and the jacket inlet temperature T_{j0}, because these are measured directly from the heat transfer medium. The dynamic model of the temperature probe of the reactor is given by the equation

$$\frac{dT_{PT100}}{dt} = \frac{T_r - T_{PT100}}{\tau_{PT100}} \tag{8}$$

where T_{PT100} is the temperature of the jacketed probe (K), and τ_{PT100} the time constant of the probe (s).

The heavy construction of the gear pump causes time dealy to the temperature of the pump head. There will be a heat flux from the pump head to the jacket when fast changes occur in the jacket temperature. The dynamic model of the temperature of the gear pump head is given by

$$\frac{dT_p}{dt} = \frac{T_j - T_p}{\tau_{Tp}} \tag{9}$$

where T_p is the temperature of the head of the gear pump (K) and, τ_{T_p} the time constant of the head of the gear pump (s).

Some of the model parameters depend on the experimental conditions. These are presented in the first column of Table 1. The parameters which need to be determined

Table 1
Classification of model parameters

Model parameters set by conditions	Constant model parameters	Model parameters dependent on variables	Variables
$\dot{Q}_r$, $\dot{Q}_c$, $\dot{Q}_{diss}$ $\dot{m}$, T_w, A	$\Sigma(mc_p)_r$, $\Sigma(mc_p)_j$ $\Sigma(mc_p)_e$, τ_{PT100}, τ_{T_p}	$\dot{Q}_{elect}$, $\dot{Q}_{pump}$, c_p, U, K_p	T_r, T_j, T_{j0}, T_{PT100} T_p

during the characterization of the apparatus are listed in the second column of Table 1. Before the set of differential equations can be solved, equations must be written describing how the model parameters depend on the model variables. The dependent parameters are presented in the third column of Table 1.

4.2. Parameter estimation

Model parameters $\Sigma(mc_p)_r$, $\Sigma(mc_p)_j$, $\Sigma(mc_p)_e$, τ_{PT100}, τ_{T_p}, $\dot{Q}_{elect}$, $\dot{Q}_{pump}$, c_p, K_p and U are unknown and various experiments were carried out to estimate them. Equations showing how the model parameters depend on the model variables are given.

4.3. Power input by the electrical heater

Four electrical resistances, each of 500 W, were mounted in the electrical heater. The thyristor unit was controlled by different analogue inputs in the determination of the power input of the electrical heater. Characterization was done with $\dot{m} = 80\ \mathrm{kg\ h^{-1}}$ and recorded as a thermogram assuming steady conditions

$$\dot{Q}_{elect} = \dot{m}(c_{pT_{j0}} T_{j0} - c_{pT_w} T_w) \tag{10}$$

Heat losses from the pipe between the jacket inlet temperature T_{j0} and the temperature after the heat exchanger T_w were neglected because there was no temperature difference between T_{j0} and T_w when the electrical heater was not used. The heat capacity of the heat transfer medium was calculated according to Eq. (11) (T_{j0} in °C)

$$c_p = 1.639\,(\mathrm{kJ\ kg^{-1}\ K^{-1}}) + 0.00439\,(\mathrm{kJ\ kg^{-1}\ K^{-1}\ °C^{-1}})\,T_{j0} \tag{11}$$

The response of the electrical heater to the analogue input was characterized with a 9th-order polynomial function according to

$$\dot{Q}_{elect} = a + bu + cu^2 + du^3 + eu^4 + fu^5 + gu^6 + hu^7 + iu^8 + ju^9 \tag{12}$$

The behaviour of the electrical heater is shown in Fig. 5; it was almost linear over the analogue input range 2.0–6.0 V, the normal operating environment.

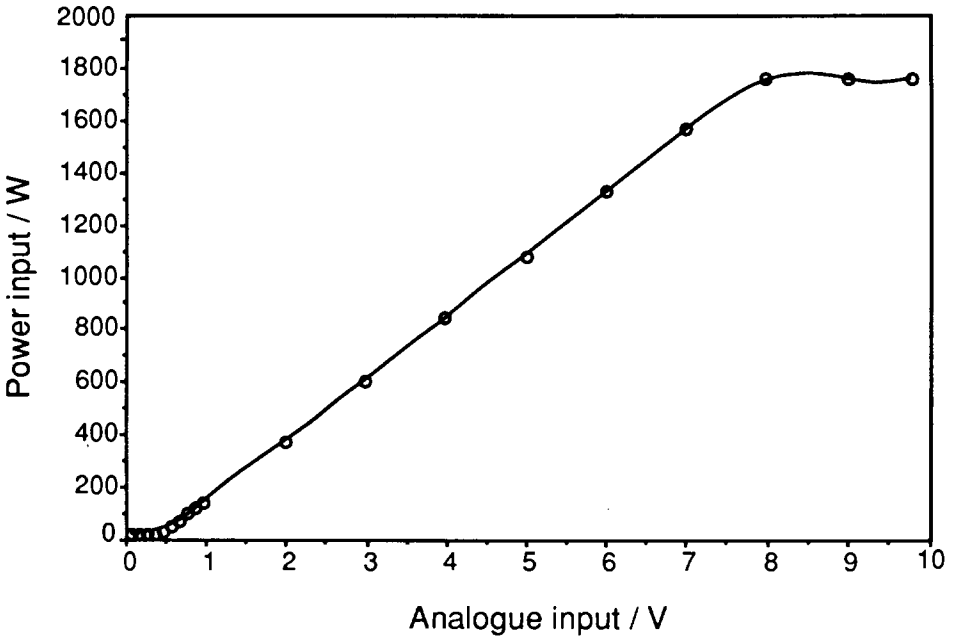

Fig. 5. Characteristic curve of the electrical heater.

4.4. *Heat capacity of the electrical heater*

The electrical heater was designed to have as small a heat capacity as possible. The dynamic response of the jacket inlet temperature to the power input from the electrical heater is shown in Fig. 6. In the characterization, the power input of the electrical heater was set to 1000 W and the heater was switched on after 2.5 min.

Eq. (7) was used to estimate the heat capacity of the electrical heater. The dT_{j0}/dt term was calculated by first computing an interpolating polynomial that passes through the surrounding points. The coefficients of that polynomial were then used in an analytical derivative of that polynomial. Evaluating the polynomial derivative at the desired data point gave an estimate of the derivative of the data set at that point. The heat capacity (1120 J K^{-1}) of the electrical heater was adjusted to minimize the sum of the squares of the differences between the dT_{j0}/dt term and the right-hand side of Eq. (7).

4.5. *Heat transfer properties in characterizations*

Heat transfer properties were determined with a blade impeller (80.0 mm, $d/D = 0.727$) over a range of stirrer speeds, from 1.67 to 10 s^{-1}. Water was employed in the reactor when determining the sum of the thermal resistances of the wall and the heat transfer medium on the jacket side (Ψ).

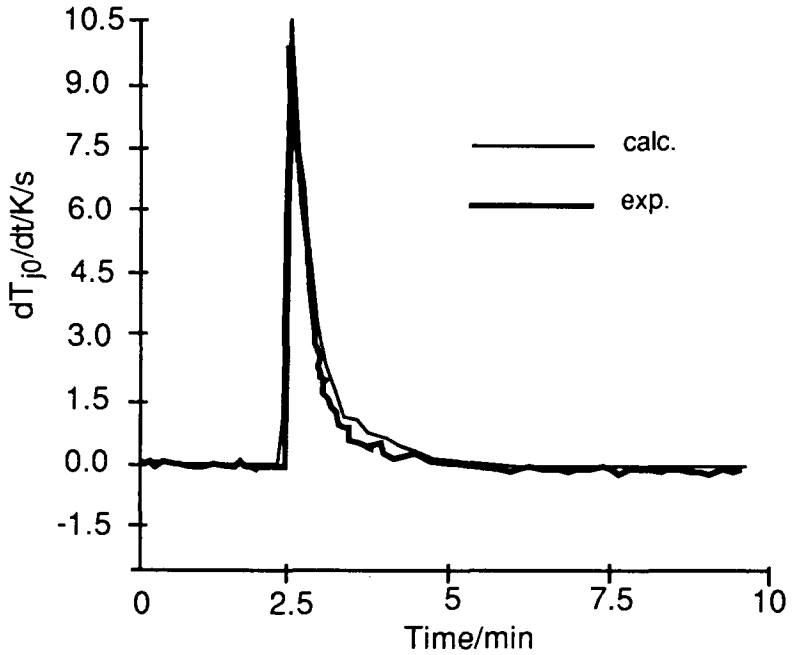

Fig. 6. Dynamic response of the jacket inlet temperature to the power input.

The relationship between the film and overall heat transfer coefficients is

$$\frac{1}{U} = \frac{1}{h_i} + \frac{s}{\lambda} + \frac{1}{h_o} \tag{13}$$

The required inside heat transfer coefficient is

$$h_i = \frac{1}{U^{-1} - \Psi} \tag{14}$$

where h_o depends on the physical properties of the heat transfer medium and, for a given flow rate, is thus a weak function of temperature; the thermal conductivity of the reactor is also somewhat temperature-dependent. Hence, during the characterization, Ψ depends on temperature, but the dependence is weak because the reactor temperature is constant; h_i depends on the stirrer speed according to [6]

$$h_i = kN^n \tag{15}$$

The Wilson [7] method was used to determine Ψ (values for s and λ are from the manufacturer of the reactor, Büchi) and, therefore, h_i was determined from measured U values at several different stirrer speeds by plotting U^{-1} against N^{-n}. The determination was made with the equation

$$\frac{1}{U} = \frac{1}{kN^n} + \Psi \tag{16}$$

For agitated reactors, n equals 2/3 in fully turbulent flow [8]. Fig. 7 shows measurements made in the calorimeter using water at three temperatures. Resistances, Ψ, for the different temperatures are presented in Table 2.

Fig. 8 summarizes the results of the heat transfer measurements over the Re range 30 000–206 000. The least squares line corresponds to

$$Nu = 0.24\mathrm{Re}^{2/3}Pr^{1/3} \tag{17}$$

$$Nu = \frac{Dh_i}{\lambda} \tag{18}$$

$$Pr = \frac{c_p\eta}{\lambda} \tag{19}$$

Analytical expression for U, h_i and h_o are shown in Table 3, below.

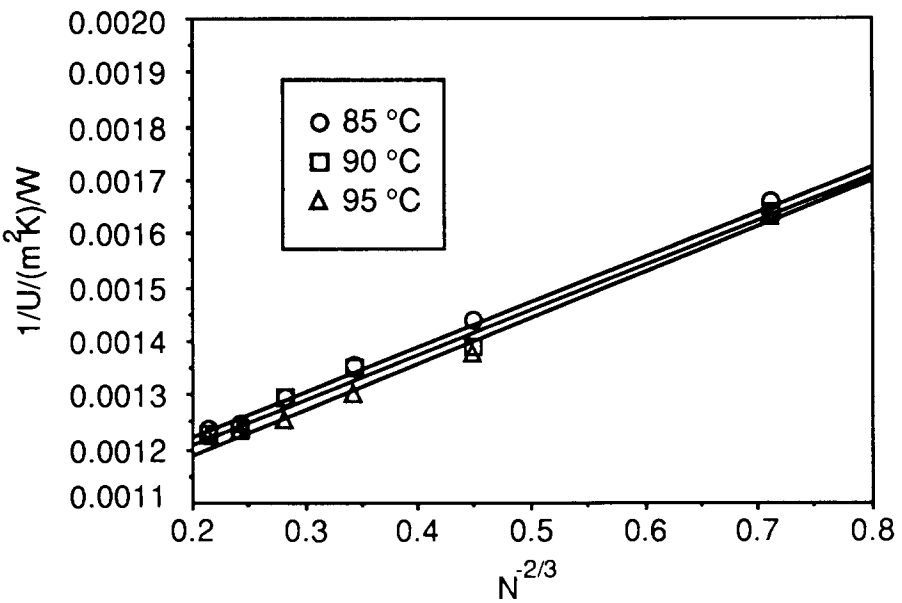

Fig. 7. Wilson plots for the blade impeller in the calorimeter.

Table 2
The heat transfer properties characterized by the Wilson method (400 rpm)

Temperature/°C	85	90	95
U/(W m^{-2} K^{-1})	745	765	790
$1/\Psi$/(W m^{-2} K^{-1})	883	900	931
h_o/(W m^{-2} K^{-1})	1149	1178	1231
h_i/(W m^{-2} K^{-1})	4767	5100	5216

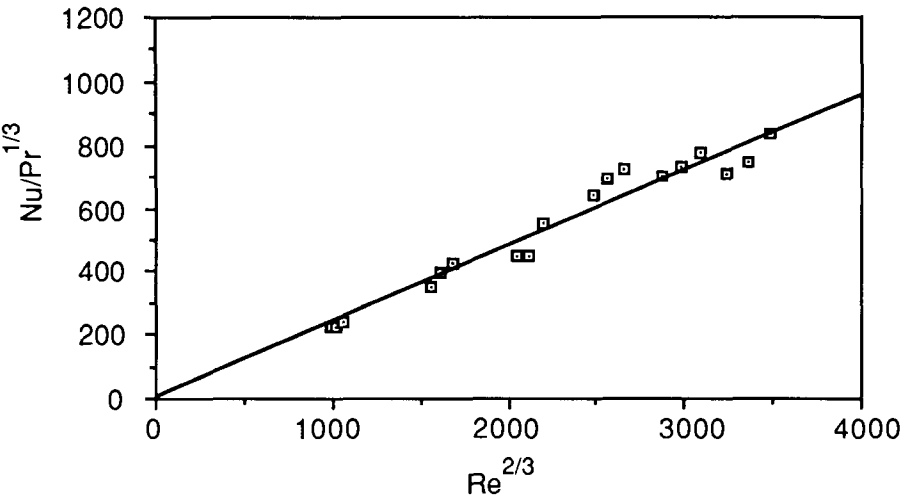

Fig. 8. Reactor side heat transfer measurements for blade impeller.

Table 3
Experimentally determined model parameters and the model equations for the calorimeter

Model parameter	Value/equation
$\Sigma(mc_p)_{const,r}$	3430 J K^{-1}
$\Sigma(mc_p)_{const,j}$	2929 J K^{-1}
$\Sigma(mc_p)_e$	1120 J K^{-1}
τ_{PT100}	13.4 s
τ_{T_p}	86 s
$\dot{Q}_{elect}$	$22.517 - 261.280u + 691.166u^2 + 460.947u^3 + 165.831u^4 - 34.138u^5 + 3.993u^6 - 0.242u^7 + 0.005u^8 + 0.0000422u^9$
$\dot{Q}_{pump}$	$107.1\,W - 0.474(W\,°C^{-1})T_j$
c_p	$1.639\,kJ\,kg^{-1}\,K^{-1} + 0.00439\,(kJ\,kg^{-1}\,K^{-1}\,°C^{-1})\,T_{j0}$
$1/U$	$\frac{1}{(\lambda/D)0.24Re^{2/3}Pr^{1/3}} + \frac{S}{\lambda} + \frac{1}{8.2(W\,m^{-2}\,K^{-1}\,°C^{-1})\,T_j + 448\,W\,m^{-2}\,K^{-1}}$
K_p	$(8.2(W\,m^{-2}\,K^{-1}\,°C^{-1})T_j + 448\,W\,m^{-2}\,K^{-1}\,0.04023\,m^2$

4.6. *Heat transfer coefficient* K_p

The heat transfer coefficient K_p is equal to the jacket-side heat transfer coefficient multiplied by the inner area of the gear pump head (0.04023 m^2, Table 3).

4.7. *Power input by the gear pump*

The power input of the gear pump was characterized with a steady state assumption and determined with the equation

$$\dot{Q}_{pump} = \dot{m}(c_{pT_j}T_j - c_{pT_{j0}}) \tag{20}$$

Fig. 9 and Table 3 summarize the results of the characterization of the gear pump.

In heat balance calorimetry, calorimetric measurements are the sum of the convective heat flow rate, the power input of the pump in the inner jacket loop, and the heat accumulation to the reactor and jacket constructions. Polymerization conditions strongly affect the accuracy of the calorimetric measurements. The accuracy of the measurement is worse when the initiator is added to the polymerization system before heating it to the polymerization temperature than when it is added at the polymerization temperature. In the latter case, there is no way to check the power input of the pump. It is essential that the power input of the gear pump can be estimated accurately. The power input of the gear pump is in the range 50–100 W, which is about three to five times greater than the heat generation rate of the reaction. If the power input is wrongly estimated, the on-line determinations of the calorimeter will not be accurate enough. Results may still be useful if recalculated with the right power input of the pump. Better sensitivity was achieved by reducing the flow rate in the inner circulation jacket loop. Although this also adversely affected the heat transfer properties of the calorimeter, some upward adjustment of the flow rate can be made when the polymerization conditions require.

4.8. *Time constant of the probe*

The reactor setpoint was changed from 90 to 93°C in the characterization of the time constant of the probe. The change was made twice: with and without the temperature probe.

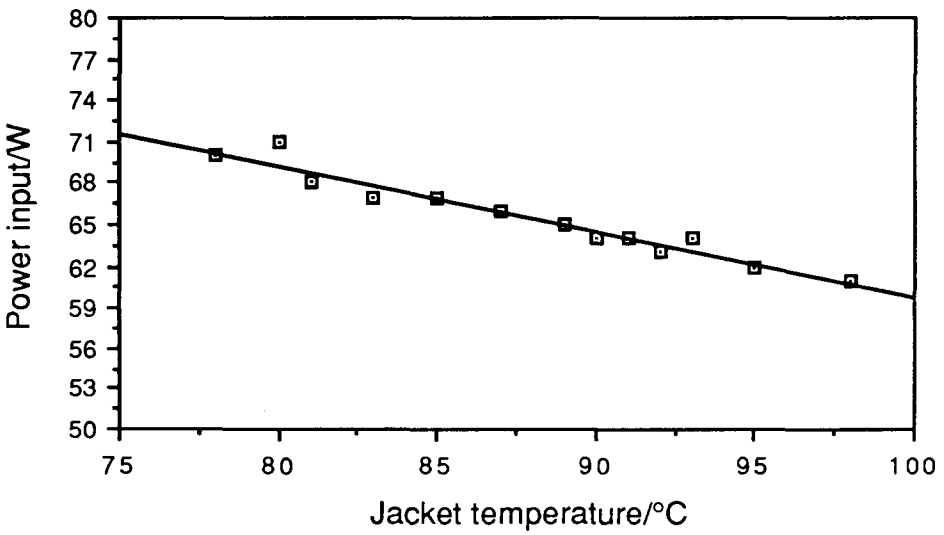

Fig. 9. Characteristic curve of power input by the gear pump.

Eq. (8) was used to estimate the time constant of the probe. The dT_{PT100}/dt term was calculated in the same way as the dT_{j0}/dt term. The time constant of the probe was adjusted to minimize the sum of the squares of the differences between the dT_{PT100}/dt term and the right-hand side of Eq. (8). Fig. 10 shows a comparison between the dT_{PT100}/dt term and the right-hand side of Eq. (8). A good fit can be seen for the value $\tau_{PT100} = 13.4$ s. The time constant is fairly large because the probe is pressure-proof.

4.9. Time constant of the heat of the gear pump

The gear pump used in the inner circulation jacket loop is of heavy construction. The construction was chosen as a compromise between good dynamic behaviour and the sensitivity of the power input of the gear pump. When the head of the gear pump is large, a high flow rate can be obtained with low rotational speed. The low speed improves the sensitivity of the power input of the pump. By contrast, a heavy construction for the gear pump adversely affects the dynamic behaviour of the jacket. The effect of the heavy construction was determined by modelling the temperature of the head of the gear pump.

A simulation reaction was used to characterize the time constant of the head of the gear pump. The dynamic response of the temperature of the head of the gear pump to this is shown in Fig. 11.

Computational procedures were similar to those used for τ_{PT100} and a value of $\tau_{T_p} = 86$ s gave a good fit (Fig. 11) between dT_p/dt and the right-hand side of Eq. (9).

4.10. Heat capacity of the jacket

A simulation reaction was also used to characterize the heat capacity of the jacket and dT_j/dt is shown in Fig. 12.

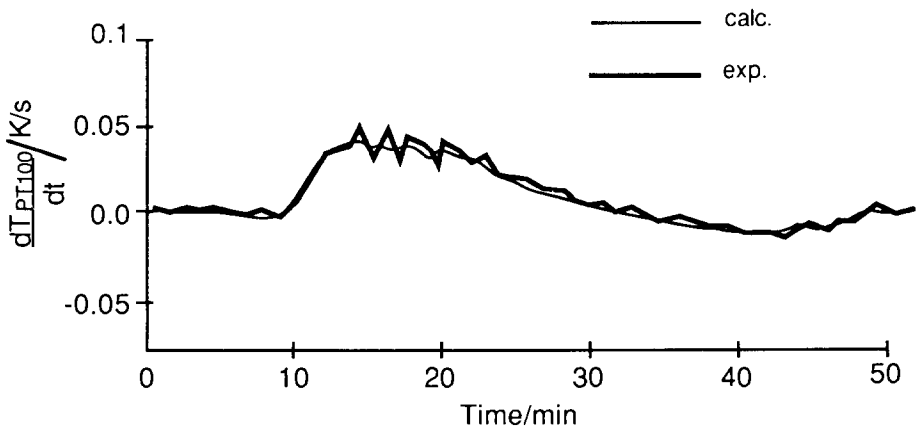

Fig. 10. Dynamic response of the temperature of the jacketed probe to change in the setpoint.

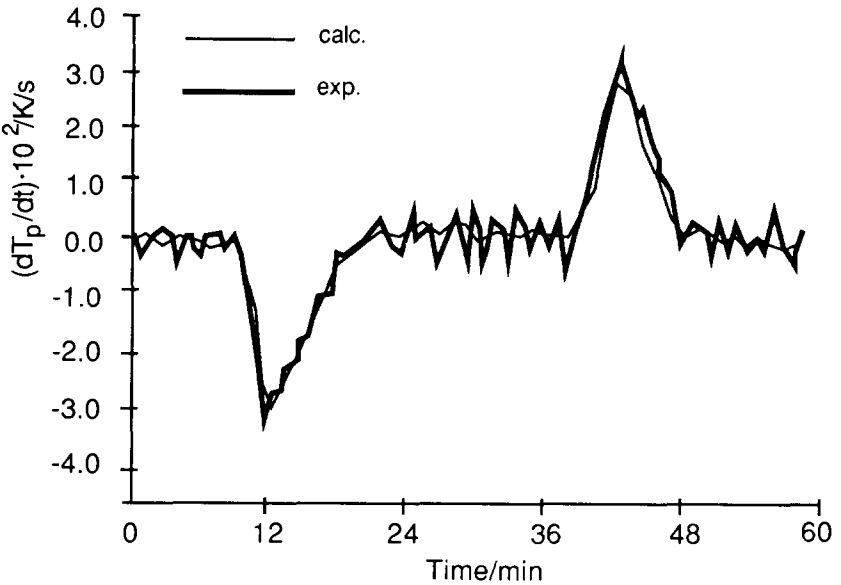

Fig. 11. Dynamic response of the temperature of the head of the gear pump in the simulation reaction. The calibration heater (50 W) was switched on after 10 min and the duration of the simulation was 30 min.

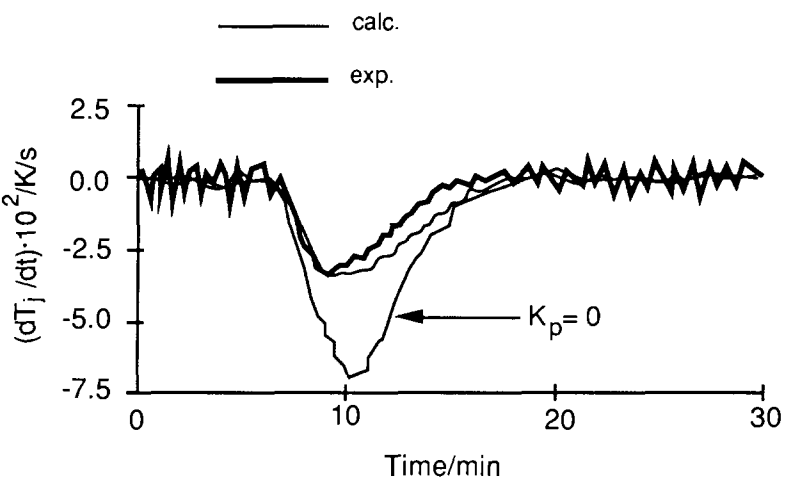

Fig. 12. Dynamic response of the temperature of the jacket in the simulation reaction. The calibration heater (50 W) was switched on after 6 min.

The heat capacity of the jacket is the sum of all heat capacities involved in the inner jacket loop. The two main factors are the heat transfer oil (0.9 kg) and the actual materials that form the jacket. The heat capacity due to the latter is the unknown parameter in the estimation. The denominator of the right-hand side of Eq. (6) is

$$\Sigma(mc_p)_j = [900(1.639 + 0.00439\,T_j) + \Sigma(mc_p)_{const,j}] \quad (21)$$

Eq. (6) was used to estimate the heat capacity of the jacket. The dT_j/dt term was calculated in the same way as the dT_{j0}/dt term. The heat capacity of the jacket was adjusted to minimize the sum of the squares of the differences between the dT_j/dt term and the right-hand side of Eq. (6). The relevant parameters ($\dot{Q}_{pump}$, K_p and U) from Table 3 were used to give the right-hand side of Eq. (6). Fig. 12 shows a comparison between the dT_j/dt term and the right-hand side of Eq. (6) for $\Sigma(mc_p)_{const,j} = 2920$ J K^{-1}. The small deviation between the model and the experiment may be due to the heat loss through the pump head. Fig. 12 also shows that the deviation between the model and the experiment becomes very large if the heat flux from the pump head to the jacket is neglected.

4.11. *Heat capacity of the reactor*

A simulation reaction was also used to characterize the heat capacity of the reactor. The dynamic response of the temperature of the reactor in the simulation is shown in Fig. 13.

The heat capacity of the reactor appears in the denominator of Eq. (5) as the sum of all heat capacities involved in the assembled reactor. These are due to the inert fluid (1.8 kg water) used and the several components of the reactor, the unknown parameter at this stage.

Eq. (5) was used to estimate the heat capacity of the reactor with the parameters of Table 3 and $\Sigma(mc_p)_{const,r}$ as the adjustable variable. Fig. 13 shows a good fit between the dT_r/dt term and the right-hand side of Eq. (5) for $\Sigma(mc_p)_{const,r} = 3430$ J K^{-1}.

The experimentally determined model parameters are collected in Table 3. The table also shows equations for determining the model parameters from the model variables.

5. Dynamic response of the calorimeter filled with an inert fluid

Water was used as an inert fluid to study the overall behaviour of the calorimeter. Experiments were preformed at 80 and 90°C. The PID parameters of the temperature

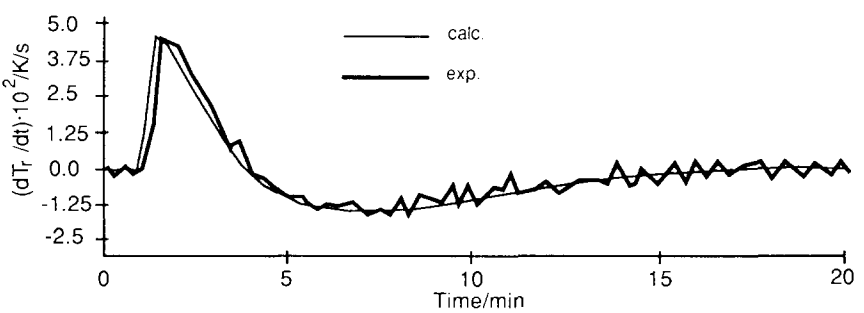

Fig. 13. Dynamic response of the temperature of the reactor in the simulation reaction. The calibration heater (50 W) was switched on after 1 min.

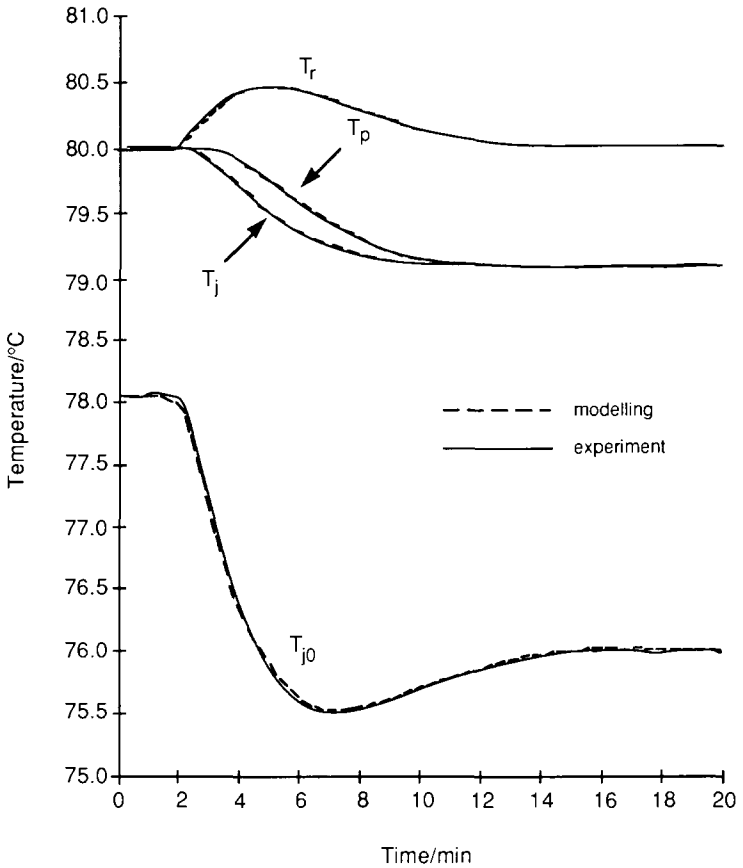

Fig. 14. Dynamic responses of the temperatures of the reactor (T_r), the jacket (T_j), the head of the gear pump (T_p) and the jacket inlet temperature (T_{j0}) in the simulation reaction. The calibration heater was switched on after 2 min and the power input of the calibration heater was set to 50 W.

control algorithm were adjusted to be quite slow to ensure that there was no oscillation in the temperature control.

Temperature responses are shown in Fig. 14. Dotted lines represent the modelling, and solid lines the experiment. In all cases there is a good fit between the two.

Comparison of T_j and T_p shows that the dynamic behaviour of the jacket is adversely affected by the heavy construction of the gear pump. It is essential to account for this by modelling the temperature of the head of the gear pump. It should be noted that Fig. 14 also shows that the characterization of the electrical heater and the temperature control algorithm used in the simulation program correspond well with the experiment. Simulations of results obtained at 90°C are equally effective.

6. Conclusion

An accurate model for the thermal effects of the reaction calorimeter is needed to ensure good estimates of basic parameters and to guarantee accurate characterization of its operation. A dynamic modelling of the reaction calorimeter makes it possible to optimize the construction of the calorimeter. It is also easier to characterize the calorimeter when a mathematical model is available. It is essential to understand the dynamic behaviour of the calorimeter before using it in determinations of real reactions. Theoretical and practical simulations allow one to find the critical parts of the calorimeter construction liable to distort results in practical use. The construction of our reaction calorimeter has a number of special features which were not easy to determine without modelling. When the heat release through the pump head was not included in the heat balance equation, the modelling was not accurate enough to be used in determinations. The time constants of the temperature measurement devices and the heat capacities must also be determined carefully to guarantee a good fit between model and experiments.

The control parameters of the calorimeter are more efficiently and easily optimized when a mathematical model is available. The control parameters need to be fitted very precisely in reaction calorimeters based on convective heat flux. These heat balance calorimeters are based on the temperature difference between the jacket inlet and outlet temperatures, where the jacket inlet temperature is the controlled variable. If the control parameters are not well characterized, there will be wide variation in the convective heat flux, which in turn will cause wide variations in the determination of the reaction.

Part 2 of this series [9] will describe the special features of polymerizations and the typical process parameters such as viscosity, heat transfer properties and heat generation for four types of polymerizations.

References

[1] H.-U. Moritz, Rechnergestützer Laborreaktor zur Emulsionspolymerisation von Vinylacetat, Habilitation Thesis TU Berlin, 1988.
[2] H.-G. Poersch-Panke, Reaktionskalorimetrie und die reaktionstechnische Untersuchung der Fällungspolymerisation von Acrylsäure, Ph. D. Thesis TU Berlin, 1991.
[3] K. Fiaty, A. Accary, C. Jallut and O. Crouslé, Thermochim. Acta, 188 (1991) 191.
[4] C. Jallut, A.-M. Crignon, G. Thomas, K. Fiaty, A. Accary and C. Chapat, Dynamic Modelling and Simulation of Batch Reactors in Computer Applications in Chemical Engineering, Elsevier, Amsterdam, 1990.
[5] W. Gerhartz, Ullmann's Encyclopedia of Industrial Chemistry, Vol. B2: Unit Operations I, VCH, Weinheim, 1988.
[6] J.R. Bourne, M. Buerli and W. Regenass, Chem. Eng. Sci., 36 (1981) 347.
[7] E.E. Wilson, A basis for rational design of heat transfer apparatus, Am. Soc. Mech. Eng., 1477 (1915) 47.
[8] V.W. Uhl, Mixing: Theory and Practice, Vol. 1, Academic Press, New York, 1966.
[9] M. Lahti, A. Avela and J. Seppälä, Polymerization calorimeter. Part 2. Practical use and application in polymerizations, Thermochim Acta, in press.